CLASSIFICATION OF PRE-BREAKDOWN PHENOMENA IN MULTICRYSTALLINE SILICON SOLAR CELLS

J.-M. Wagner, J. Bauer, O. Breitenstein
Max Planck Institute of Microstructure Physics
Weinberg 2, 06120 Halle, Germany
jmwagner@mpi-halle.mpg.de · +49-345-5582761 · Fax: +49-345-5511223

ABSTRACT: Pre-breakdown mechanisms in semiconductors exhibit characteristic temperature dependences. Using temperature-dependent lock-in thermography (LIT) measurements and electroluminescence imaging under reverse bias we have found local regions with positive and with negative temperature coefficient (TC) of the breakdown current of multicrystalline silicon solar cells. In some regions, the temperature coefficient changes sign (from negative to positive) when going to higher temperatures. At low temperatures and for moderate reverse voltages, most pre-breakdown sites show a negative temperature coefficient, whereas the total cell current increases with temperature. This contradiction is resolved by rescaling the LIT images revealing that in the whole area of the cell a homogeneous reverse current flows, which increases with temperature and thereby compensates the negative TC of the localized currents. Altogether, in addition to the hard pre-breakdown (type III), the recombination-active defect-related soft pre-breakdown (type II) and the early pre-breakdown (type I), two additional pre-breakdown phenomena have been identified.
Keywords: Electrical Properties, Lock-in Thermography, Multicrystalline Silicon, Pre-Breakdown, Shunts, Silicon Solar Cell

1 INTRODUCTION

Due to the problem of hot spots possibly occurring for unintentionally reverse-biased cells, there is a recent interest in the investigation of the pre-breakdown behaviour of multicrystalline (mc) Si solar cells. The hard pre-breakdown of standard industrial, acidically etched mc Si cells has been identified as being due to avalanche breakdown at etch pits [1], and cells with an alkaline texture also show a hard pre-breakdown but located at certain bulk-related defects [2]. The mechanisms relevant for weaker pre-breakdown phenomena, however, occurring at lesser reverse bias, are not well understood yet.

The main fundamental mechanisms responsible for the breakdown of *p-n* junctions, besides thermal breakdown at very high temperatures, are impact ionization, leading to avalanche multiplication, and internal field emission (tunnelling). Both mechanisms are possibly enhanced by material defects or impurities [3, 4], and also metal precipitates can play a certain role [5]. Avalanche breakdown is sensitive to junction curvature and doping density [6]. So far, in the literature pre-breakdown phenomena are mainly differentiated according to the slope of their current–voltage characteristic [4] or their onset voltage [7]. Since in general the physical mechanisms leading to breakdown of a *p-n* junction are distinctly dependent on temperature, a more detailed classification of pre-breakdown phenomena must also refer to their temperature dependence. Furthermore, under operation in a module, solar cells reach significantly higher temperatures than the usual laboratory temperature. In the present work we report on an extensive experimental study of the temperature behaviour of pre-breakdown phenomena in mc Si solar cells, especially for low to moderate reverse voltages where the onset of different pre-breakdown stages is found.

2 EXPERIMENTAL

The breakdown currents of an mc Si solar cell can be sensitively imaged by lock-in thermography (LIT) and electroluminescence (EL). Recently we have proposed LIT-based techniques to study the physical parameters of pre-breakdown phenomena [8]. For thermally thin samples, the –90° LIT signal taken in the dark (DLIT image) is proportional to the local heating power density and can be rescaled to represent the current density. Varying the temperature (the applied reverse voltage), the corresponding variations of the local currents can be obtained and can be expressed as relative change per kelvin (per volt), i.e. as the normalized temperature coefficient, TC, at a certain midpoint temperature (the normalized slope at a certain midpoint voltage). In our study we investigated standard industrial (156 × 156 mm^2), acidically etched mc Si solar cells free from ohmic shunts.

3 RESULTS AND DISCUSSION

3.1 Reverse current–voltage characteristic

The reverse characteristic (total reverse current vs. applied bias voltage) of a typical cell is shown in Fig. 1 for four different temperatures. In the region of weak pre-breakdown (between zero and approx. –13 V bias), the total reverse current of the investigated mc Si solar cells increases in magnitude with increasing temperature (positive TC), whereas in the hard pre-breakdown region (beyond approx. –13 V bias) the total reverse current decreases with rising temperature (negative TC). The latter behaviour usually indicates avalanche breakdown, and in a separate investigation it was indeed confirmed that the hard breakdown observed here is due to an avalanche effect occurring at the bottom of etch pits where the electric field is enhanced by the tip effect [1, 9]. The former behaviour (increase of the reverse current with increasing temperature) usually indicates tunnelling as conduction mechanism. However, direct band-to-band tunnelling (Zener effect) occurs only for very narrow depletion regions, requiring a very high doping, which is not reached here. Therefore, the weak pre-breakdown has to be investigated in more detail.

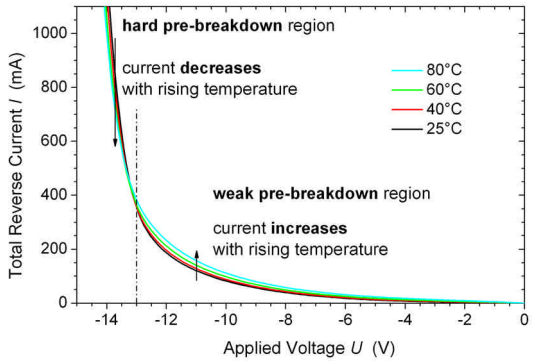

Figure 1: Reverse-bias current–voltage characteristic of a typical acidically etched mc Si solar cell for four different temperatures.

3.2 Dark lock-in thermography (DLIT)

Since junction breakdown can be defect-assisted [3, 4], it has to be checked for a possible correlation of the weak pre-breakdown sites with material defects. To that end, a series of room-temperature LIT images taken in the dark (DLIT) is recorded for varying bias, the results being shown in Fig. 2.

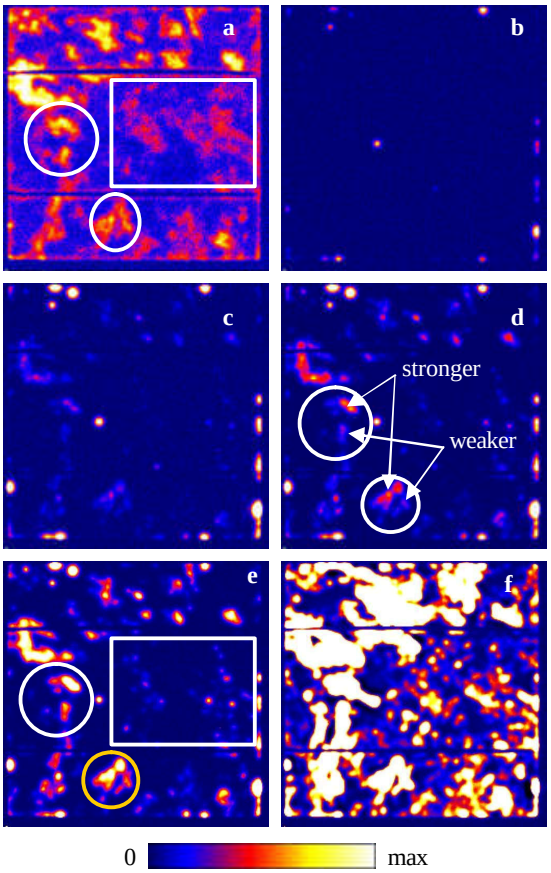

Figure 2: A series of DLIT images of the cell investigated in Fig. 1, taken for bias voltages of +0.6 V (a), –5 V (b), –8 V (c), –10 V (d), –12 V (e), and –14 V (f). The scaling bar represents temperature differences from zero to 2 mK (a), 0.5 mK (b), 5 mK (c), 10 mK (d), and 15 mK (e, f), respectively.

The DLIT signal observed for a forward bias nearly equal the open-circuit voltage (where the local heating of the cell is due to the diffusion current, Fig. 2a) is directly correlated with recombination-active defects [9]. The first observable DLIT signals under reverse bias, occurring at about –5 V, are mainly located at the edge or at isolated sites inside the cell area (Fig. 2b). They are not correlated with recombination-active defects. This corresponds to the "stage-I" pre-breakdown onset described by Kwapil et al. [7]. The origin of this pre-breakdown (also called "type-I" pre-breakdown [10]) is unclear; it has an almost linear reverse-bias current–voltage (*I–U*) characteristic [11]. From a bias of about –8 V on, defect-related "stage-II" pre-breakdown onset is observed in regions of recombination-active defects (Figs. 2c,d,e). This is a different type of breakdown ("type II"), it has a soft-exponential characteristic [11]. As "stage-III" onset at even higher voltages, hard pre-breakdown occurs at newly appearing sites (not correlated with recombination-active defects), and the current at all stage-I and stage-II sites increases (Fig. 2f). Due to its hard-exponential characteristic [11], the hard pre-breakdown dominates the total reverse *I–U* characteristic. So far, the origin of this "type-III" breakdown has only been identified for acidically etched mc Si cells [1, 9].

Two important facts can be noticed from Fig. 2: First, there is no complete correlation between the stage-II pre-breakdown sites and the recombination-active defects, since there are large regions in Fig. 2a indicating somewhat weaker diffusion currents, but nearly no or only very little breakdown currents are found there for biases up to –12 V (see white rectangle). Interestingly, in the latter regions a strong forward-bias electroluminescence signal at 1555 nm can be found [12]. Second, there are defect regions showing a similar strength of their diffusion currents but leading to either higher or lower reverse currents at a given bias (see circles). Therefore, defect-related stage-II pre-breakdown onset seems to comprise at least two different kinds of pre-breakdown sites, stronger and weaker ones (cf. Fig. 2d); this will be further discussed below. Here, all stage-II sites show only rather weak 1555 nm luminescence [12]. However, this is not generally the case; in a recent study, both type-II breakdown and sub-band-gap luminescence were found in the same region of an alkaline-textured solar cell [13].

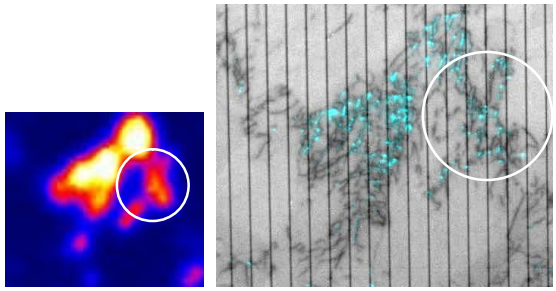

Figure 3: The left image shows the region marked by the yellow circle in Fig. 2e. The right image shows the corresponding region, imaged by EL under forward and reverse bias, as an overlay of both EL signals; grey: forward bias, cyan: reverse bias (–12 V). The dynamic of the reverse-bias signal has been reduced to make (slightly) visible also its weakest parts.

3.3 Electroluminescence (EL)

There are several possibilities why, despite of equal diffusion currents, the breakdown currents differ at the

areas marked with circles in Fig. 2. First, there could be a varying concentration of microscopic breakdown sites (of otherwise identical properties). Second, there could be similar numbers of microscopic breakdown sites, but with varying strength. Third, the reason could be a varying onset voltage of the pre-breakdown, as it is the case for avalanche breakdown (where it depends on junction geometry [6]); this could be a reason behind possibility #2. Finally, there could be different breakdown mechanisms at play.

To find out what it is like here, we have used EL imaging under forward and reverse bias, both images taken with the same set-up directly after one another. For the region marked by the yellow circle in Fig. 2e, the result is shown as an overlay image in Fig. 3 (right). As expected, the reverse-bias EL signal originates from positions of (or close to) recombination-active defects, the latter showing up as darker elements in the forward-bias EL image. Also shown is an enlarged part of the corresponding DLIT image, Fig. 2e, where the region of weak DLIT signal is indicated by a white circle (left part of Fig. 3). It can be seen that in the region of weak DLIT signal, the reverse-bias EL signal consists of fewer spots (but of similar strength) than are found in the other parts of the defect region. A closer inspection reveals that in the "weaker" region, there are mainly isolated EL spots, whereas in the "stronger" region, they are frequently arranged in form of densely-occupied lines. Thus, there is a difference in concentration of microscopic pre-breakdown sites.

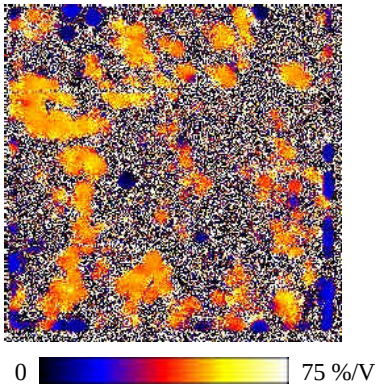

Figure 4: Slope-DLIT image of the cell shown in Figs. 1 and 2, taken at room temperature and a midpoint voltage (voltage difference) of –11 V (2 V).

For checking the voltage dependence, we have used a room-temperature Slope-DLIT [8] investigation; the result for a midpoint voltage of –11 V is shown in Fig. 4. A Slope-DLIT image shows the normalized gradient (or, in other words, the relative variation) of the *I–U* characteristic. Since each breakdown type has a specific *I–U* characteristic, in each voltage range there is also a specific slope. Therefore, for a given reverse bias, cell areas with the same slope exhibit the same breakdown mechanism. (Of course this does not hold for those specific voltages where the slopes corresponding to different breakdown mechanisms are identical; then, one needs to check again at slightly varied voltages.) Early pre-breakdown (type I) leads to a minor slope. All spots in Fig. 4 which are blue can therefore be identified as type-I breakdown sites. Since the Slope-DLIT image is normalized, its result is independent of the local current strength. Therefore it is easier to locate all early pre-breakdown spots in the Slope-DLIT image than in an DLIT image taken at low reverse bias (compare Fig. 4 with Fig. 2b). On the same basis, all regions of Fig. 4 which show an orange colour can be identified as type-II breakdown sites, since this breakdown mechanism has a soft-exponential *I–U* characteristic and therefore dominates the slope in this voltage range. In particular, this means that there are no different breakdown mechanisms at play in the "weaker" and "stronger" regions discussed above.

3.4 Temperature dependence

To investigate in detail the temperature dependence of the reverse current shown in Fig. 1, we have taken DLIT images at several bias values and for varying temperature. Using our method as described in Ref. 8, these images were transformed into normalized temperature-coefficient DLIT (TC-DLIT) images. Figs. 5a–c show the results for –10 V bias, Fig. 5d for –14 V. In these images, regions with nearly vanishing, noisy DLIT signal have been blanked. From this procedure it is clear that only those regions lead to a "signal" in the TC-DLIT image, which have been observed as pre-breakdown sites in Fig. 2d.

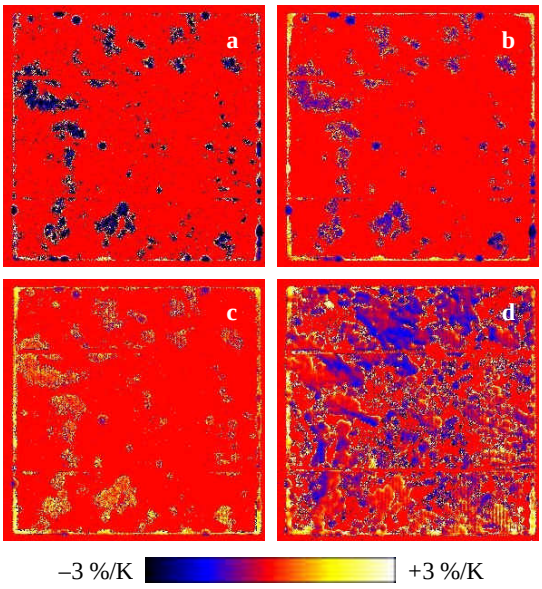

Figure 5: A series of TC-DLIT images of the cell shown in Figs. 1 and 2, taken at a fixed bias voltage of –10 V and midpoint temperatures (temperature differences) of 32.5 °C (15 K) (a), 50 °C (20 K) (b), 70 °C (20 K) (c), as well as at –14 V and 70 °C (20 K) (d). Regions with nearly vanishing signal are blanked to zero %/K (red).

With respect to increasing temperature, three important observations can be made from Fig. 5. First, while for the stage-I pre-breakdown sites the temperature coefficient becomes less negative only slightly, the temperature coefficient of all stage-II pre-breakdown sites (both strong and weak ones) is equal and varies from being negative at low temperatures to being close to zero or becoming even positive at higher temperatures. This could mean that at the latter sites not only the defect-assisted breakdown mechanism (possibly trap-assisted avalanche) is relevant for the magnitude of the breakdown current but additionally another, strongly temperature-

dependent conduction (injection) process is involved. Alternatively it could mean that the type of the breakdown mechanism changes at higher temperatures; at least for highly defect-rich areas, hopping conduction would be plausible [14, 15]. Unfortunately, so far no further experimental insight is available. Interestingly, this sign reversal of the temperature coefficient is not found for the hard pre-breakdown sites which at any temperature show a negative TC (Fig. 5d; see also Ref. 15).

Second: Although hardly noticeable as a contribution to the pre-breakdown current in Fig. 2, besides the stage-I pre-breakdown sites located at the edge, nearly the whole edge of the cell shows up in the TC-DLIT images as a pre-breakdown "region" of its own, showing a positive TC. This illustrates the advantage of the normalized TC-DLIT evaluation procedure which shows relative current change, independent of the absolute magnitude of the respective current.

Third: At low temperature the TC of the reverse current at the pre-breakdown sites is negative, in clear contrast to the positive TC of the total reverse current (Fig. 1). Just some of the edge currents show a marked increase with temperature. However, these currents are too weak to account for the overall current increase. This contradiction can be resolved by rescaling the DLIT images underlying Fig. 5 to make visible the nearly vanishing, noisy signal discarded in Fig. 5 by blanking. These images are shown in Fig. 6.

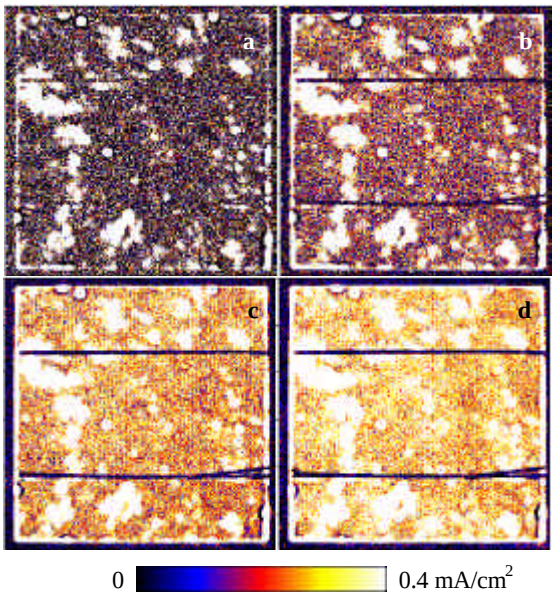

Figure 6: The series of DLIT images underlying Fig. 5a–c (rescaled according to Ref. 8 to represent current density images), taken at a bias voltage of –10 V and temperatures of 25 °C (a), 40 °C (b), 60 °C (c), and 80 °C (d).

It can be seen that the weak current flowing in the cell area outside the localized pre-breakdown sites (which appear completely white in Fig. 6) increases with temperature and therefore can not be ignored for the discussion of the temperature behaviour of the total reverse current. This current can be included in the TC-DLIT images when they are shown without the blanking, which is done in Fig. 7. The nature of this current is unclear; the saturation current J_0 (typ. 1 pA/cm^2 at room temperature) still is to be expected about 6 orders of magnitude smaller at 80 °C .

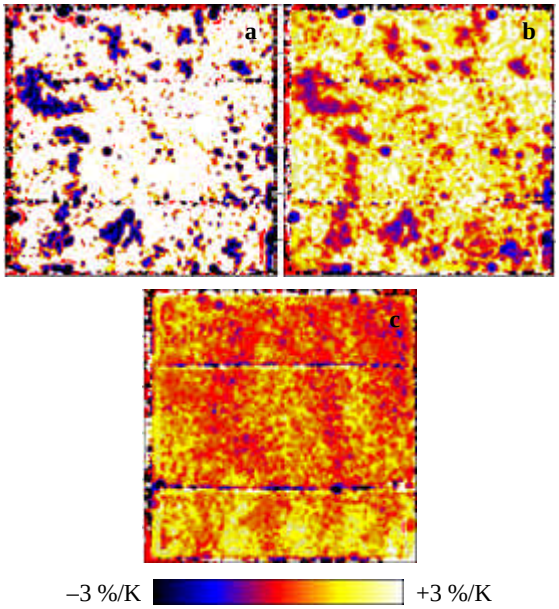

Figure 7: The same series of TC-DLIT images as shown in Fig. 5a–c [bias voltage –10 V, midpoint temperatures (temperature differences) 32.5 °C (15 K) (a), 50 °C (20 K) (b), and 70 °C (20 K) (c)], but without the blanking; 3×3 pixel binning was applied to reduce the noise.

Here it can be seen that most parts of the TC-DLIT images show a strongly positive TC of the pre-breakdown current, in accordance with the positive TC of the total reverse current (Fig. 1). This means that in the temperature range under investigation, the total reverse current to a substantial, non-negligible part consists of the large-area current just described and is therefore not representative of the localized pre-breakdown currents. This holds especially at the slightly elevated temperatures of solar cell operation in a module. However, at lower temperatures, when the large-area current is sufficiently suppressed, the measured total reverse current originates from the localized pre-breakdown sites only.

4 SUMMARY AND CONCLUSIONS

Altogether, in addition to the hard pre-breakdown (type III; occurring beyond –13 V bias), the recombination-active defect-related soft pre-breakdown (type II) and the early pre-breakdown (type I), two additional pre-breakdown phenomena have been identified: a minor leakage current at the cell edge, which shows a positive TC for all temperatures, and the positive-TC large-area current which dominates the total reverse current. Further, it was found that the "early" pre-breakdown (type I) current shows a negative TC that slightly becomes less negative for increasing temperature, whereas the TC of the soft pre-breakdown (type II) current changes sign. It is negative only for low temperatures but becomes zero or even slightly positive for higher temperatures. There is no difference in the breakdown mechanism of stronger and weaker stage-II breakdown sites; at both, type-II pre-breakdown takes place.

Note that not all recombination-active defects lead to stage-II onset sites (cf. the large rectangle in Figs. 2a,e). As can be seen in Fig. 2f, they start to break down at

significantly higher reverse voltages; only these show a pronounced 1555 nm luminescence. The simultaneous presence of this luminescence and the slightly lesser diffusion current compared to other recombination-active regions point to the fact that at these defects, additional traps that could lead to non-radiative recombination are not present.

On the other hand, the type-II pre-breakdown regions exhibit no 1555 nm luminescence, an increased diffusion current, and different concentrations of microscopic breakdown sites are found in regions of stronger or weaker type-II pre-breakdown. The latter facts points to the possibility that the same kind of recombination-active defect, in order to also act as a breakdown site, is somewhat modified by additional contaminations. This modification is not per se present at all such defects. In other words, a recombination-active defect free from 1555 nm luminescence is not necessarily a breakdown site. This has to be investigated further.

Acknowledgment: This work was financially supported by the German Federal Ministry for the Environment, Nature Conservation and Nuclear Safety (BMU) and all the industry partners within the research cluster SolarFocus (contract 0327650 D; www.solarfocus.org). The content of this publication is the responsibility of the authors

REFERENCES

[1] J. Bauer, J.-M. Wagner et al., phys. stat. sol. RRL **3** (2009) 40
[2] D. Lausch, K. Petter et al., phys. stat. sol. RRL **3** (2009) 70
[3] A. G. Chynoweth and G. L. Pearson, J. Appl. Phys. **29** (1958) 1103; R. Lal and R. Sharan, Solid-State Electronics **29** (1986) 1015; A. Schenk, Solid-State Electronics **36** (1993) 19
[4] S. Mahadevan, S. M. Hardas, G. Suryan, phys. stat. sol. (a) **8** (1971) 335
[5] A. Goetzberger and W. Shockley, J. Appl. Phys. **31** (1960) 1821
[6] S. M. Sze and G. Gibbons, Solid-State Electron. **9** (1966) 831; D. V. Speeney and G. P. Carey, Solid-State Electron. **10** (1967) 177
[7] W. Kwapil, M. Kasemann et al., Proc. 23rd EU-PVSEC, Valencia (2008) 1797
[8] O. Breitenstein, J. Bauer et al., Prog. Photovolt: Res. Appl. **16** (2008) 679
[9] J.-M. Wagner, J. Bauer et al., Proc. 23rd EU-PVSEC, Valencia (2008) 1164
[10] W. Kwapil, M. Kasemann et al., to appear in J. Appl. Phys. (2009)
[11] M. Kasemann, W. Kwapil et al., Proc. 23rd EU-PVSEC, Valencia (2008) 965
[12] M. Kasemann, W. Kwapil et al., Proc. 33rd IEEE-PVSC, San Diego (2008), No. 148
[13] K. Bothe, D. Hinken et al., Proc. 24th EU-PVSEC, Hamburg (2009) N.N. (this volume)
[14] O. Breitenstein, P. Altermatt et al., Proc. 21st EU-PVSEC, Dresden (2006) 625;
[15] O. Breitenstein, J. Bauer et al., Superlatt. Microstruct. **45** (2009) 182